Three-Dimensional Aerodynamic Design Optimization of a Turbine Blade by Using an Adjoint Method

Jiaqi Luo[1]
e-mail: jiaqil@uci.edu

Juntao Xiong

Feng Liu
e-mail: fliu@uci.edu

Department of Mechanical and Aerospace Engineering,
University of California, Irvine,
Irvine, CA 92697-3975

Ivan McBean
Alstom Power (Switzerland),
Baden 5401, Switzerland

This paper presents the application of an adjoint method to the aerodynamic design optimization of a turbine blade. With the adjoint method, the complete gradient information needed for optimization can be obtained by solving the governing flow equations and their corresponding adjoint equations only once, regardless of the number of design parameters. The formulations including imposition of appropriate boundary conditions for the adjoint equations of the Euler equations for turbomachinery problems are presented. Two design cases are demonstrated for a turbine cascade that involves a high tip flare, characteristic of steam turbine blading in low-pressure turbines. The results demonstrate that the design optimization method is effective and the redesigned blade yields weaker shock and compression waves in the supersonic region of the flow while satisfying the specified constraint. The relative effects of changing blade profile stagger, modifying the blade profile shape, and changing both stagger and profile shape at the same time are examined and compared. Navier–Stokes calculations are performed to confirm the performance at both the design and off-design conditions of the blade designed by the Euler method. [DOI: 10.1115/1.4001166]

1 Introduction

In recent years, research and application of aerodynamic design optimization (ADO) technology based on computational fluid dynamics (CFD) have become very active. There are a number of different strategies with a range of effectiveness and different levels of computational effort [1]. Compared with the long hours of manual iteration typically found in the turbine design process, optimization can be executed by an automatic computer procedure based on advanced optimization theory and thus allow the designer to focus on achieving an optimal flow structure and blade performance.

In general, a typical ADO program consists of two main components: a flow solver and an optimizer. The flow solver is used to analyze the flow field and evaluate aerodynamic performance. The optimizer is used to identify how to change the geometry to achieve a particular thermodynamic objective. An essential part of developing a gradient-based optimization method is to find a fast and accurate way to calculate the gradient information because it is the most time-consuming part in the whole design process. Although a variety of traditional approaches, such as response surface methodology [2,3] and finite difference methods [4], are still widely used in ADO problems, developing more efficient and accurate optimization methods is of high priority to designers because the computational effort for the traditional methods is proportional to the number of design parameters and thus very costly when the number of design parameters is large.

An alternative way is the adjoint approach advocated by Jameson [1,5]. This method eliminates the explicit dependence of gradient information on the variation of the flow field through the use of the adjoint equations to the original flow equations. The solution of the adjoint equations is on the same level of effort as one flow solution. By solving the Euler/Navier–Stokes (NS) equations and their corresponding adjoint equations only once, one can obtain the complete gradient information needed for optimization

independent of the number of design parameters. Jameson and co-workers [1,5–7] performed aerodynamic design optimization for airfoils, wings, and wing-body combinations. The adjoint method has been subsequently used for the design and optimization of many complex configurations for external flows. However, at present, there are only a few reported applications of the adjoint method for the design and optimization of turbomachinery blades, for example, Refs. [8–15].

Compared with the external flow over aircraft wings, turbomachinery flow is much more complex because of the complex internal geometry, the relative motion of the blades, and the multistage configuration of the machine. There are many distinct aspects of the design of turbomachinery blades that have not been studied before, including the proper choice and implementation of objective functions, constraints, design parameters, and boundary conditions. For example, an important aspect for turbomachinery is the specification of thermodynamic constraints on a blade row or stage as dictated usually by a one-dimensional through-flow design of the complete compressor or turbine system, which is usually separately optimized in the preliminary design. One may choose the total to static pressure ratio and swallowing capacity as constraints and allow the row or stage loading to change due to changes in the blade shape. Alternatively, one may fix the total to static pressure ratio and the row or stage loading but allow changes in the swallowing capacity. The design process should not allow any excess freedom that can lead to false performance improvement because of unintended changes in the one-dimensional thermodynamics rather than a true improvement in the performance of the blade design at the given particular thermodynamics for the row or stage.

The present paper attempts to develop the adjoint approach for the design and optimization of turbomachinery blades, in particular, to address the above mentioned issues. We present unique formulations of the objective functions, constraints, and design parameters that are suitable and effective for turbomachinery blade rows. The inlet and outlet boundary conditions for turbomachinery flows lead to special boundary conditions for the adjoint equations. The different boundary conditions and the gradient formulas corresponding to the different design objectives are derived and presented for the Euler equations. The inter-relations of the objective functions, the constraints, and the design parameters are
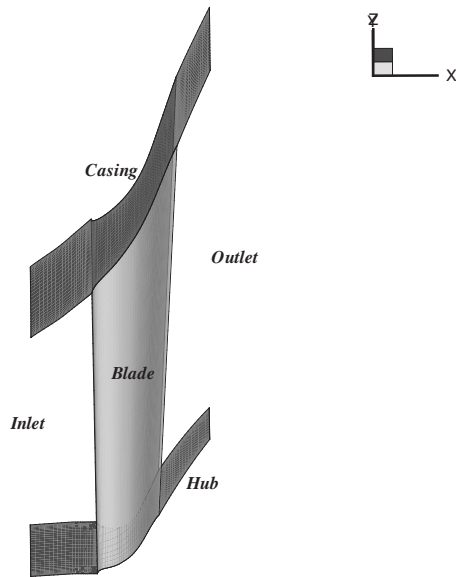

Fig. 1 Configuration of a typical low-pressure turbine stator

studied for the success of the design. One significant contribution of this work is the development and use of a restaggering method of the blade profiles coupled with modification of the blade profiles. Such a combined approach not only reflects the practice of the industry but also is shown here to be critical for obtaining better performance. A simple profile change without changing stagger or a change in stagger without modification of the profile is shown to be not sufficient to bring an improved design within the given thermodynamic constraint. The details of the mathematical formulation and the method to restagger and modify the blade profiles for an annular blade row are presented in Sec. 2.

Section 3 demonstrates the ability of the proposed formulations of the adjoint method to design and optimize a typical turbine blade row. Two cases are considered. The first is an example of inverse design by use of the optimization method, where a proper spanwise distribution of blade stagger angle is sought to achieve a given spanwise distribution of pitch-averaged exit flow angle. The second case seeks the redesign of the blade by changing both the local stagger angle as well as the blade profile to minimize the total pressure loss. Two different constraints are considered: averaged flow turning and mass flow rate. Both the inverse design and the performance optimization cases are shown to be very effective in achieving the design objectives while satisfying the constraints. Finally, the designed blades in the second case are checked for their performance at off-design conditions by both Euler and Navier–Stokes computations to assess the robustness of the design.

2 Description of Optimization Problem

We apply our optimization method to a typical turbine blade row. Figure 1 shows the geometry of the case considered. This is typical of a stator blade found in a low-pressure steam turbine in terms of the pitch to chord ratio over the blade span, the exit angle, the flat-backed profile sections, and the high flare angle at the tip of the blade. At the blade hub, the contour is at a constant radius. The flow over the blade is usually transonic; the exit Mach number is above unity over most of the blade span.

The design optimization is performed at the same design conditions. At the inlet, the total pressure, total temperature, and inflow angles are specified. At the outlet, the exit static pressure corresponding to an isentropic Mach number of 1.16 is specified.

At the outset of a design optimization task, one has to define three sets of variables or functions: (1) the design objective or cost function to be minimized; (2) the design space, usually in the form

of design parameters that specify the geometry of the blade; and (3) any design constraints on the geometry or the flow. The choice of the above functions and the basic principles of the adjoint method will be discussed in Secs. 2.1–2.3.

2.1 Choice of the Cost Function. In the present work, two types of cost functions are used. In the first, we strive to design the blade such that the pitch-averaged flow angle at the exit of the blade row attains a specified distribution. Very often the designer may have a desired spanwise distribution of the flow angle and would like to achieve that by restaggering the blade profiles while maintaining the same averaged turning. This is an inverse design problem. We can always convert such an inverse design problem to an optimization problem by defining a cost function that measures the absolute or least-squares error of the designed flow angle distribution from the desired distribution. We define the following least-squares error as the cost function:

$$I = \frac{1}{2} \int [\bar{\beta}(r) - \bar{\beta}_0(r)]^2 dr \qquad (1)$$

where the integration is done from hub to tip at the exit cross section of the blade passage, $\bar{\beta}(r)$ is the circumferentially averaged flow angle at a given radial location r, and $\bar{\beta}_0(r)$ is the specified target flow angle distribution.

The second type of objective functions involves cost functions that directly measure a performance parameter of interest of the turbomachinery blade row. One might choose to maximize the total exit to inlet pressure ratio or the adiabatic efficiency. An equivalent and perhaps more general approach is to minimize the mass-averaged entropy generation across a blade row. Thus, we choose

$$I = s_{gen} = \frac{\int_{B_o} s \rho u_j N_j dA}{\int_{B_o} \rho u_j N_j dA} \qquad (2)$$

where B_o indicates the exit boundary of the blade row, and dA is the differential area.

The formulations of the adjoint equations and their boundary conditions corresponding to the Euler equations for turbomachinery problems are discussed below.

2.2 The Adjoint Equations and Boundary Conditions. Recognizing its dependence on the flow field solution W and the geometry of the blade row $\mathcal{F}$, we write the cost function in either Eq. (1) or Eq. (2) in the following general functional form:

$$I = I(W, \mathcal{F}) \qquad (3)$$

A direct application of variation principle to Eq. (3) yields

$$\delta I = \left[\frac{\partial I}{\partial W}\right] \delta W + \left[\frac{\partial I}{\partial \mathcal{F}}\right] \delta \mathcal{F} \qquad (4)$$

The first and the second terms on the right-hand-side of the equation represent the changes due to the variation of flow field and that of the geometry, respectively. The variation of the flow field δW depends implicitly on the variation of the geometry $\delta \mathcal{F}$ through the governing flow equations, such as the Euler or the Navier–Stokes equations, which may be generally represented by the following functional form:

$$R(W, \mathcal{F}) = 0 \qquad (5)$$

The geometry of the blade row $\mathcal{F}$ in principle is described by continuous functions and therefore contains an infinite number of parameters although very often $\mathcal{F}$ is replaced with a finite albeit large number of discrete design parameters. A direct evaluation of δW with respect to $\delta \mathcal{F}$ involves repetitive solution of the governing flow equations and thus is very time consuming if not prohibitive for large numbers of design parameters even when a simplified surrogate model is used in place of the original flow equations. The key of the adjoint-equation method is to eliminate

the need for directly computing δW. Taking the variation of Eq. (5), we obtain

$$\delta R = \left[\frac{\partial R}{\partial W}\right]\delta W + \left[\frac{\partial R}{\partial \mathcal{F}}\right]\delta \mathcal{F} = 0 \qquad (6)$$

Multiplying Eq. (6) by a Lagrange multiplier Ψ^T and then subtracting it from Eq. (4), we obtain

$$\delta I = \left\{\left[\frac{\partial I}{\partial W}\right] - \Psi^T\left[\frac{\partial R}{\partial W}\right]\right\}\delta W + \left\{\left[\frac{\partial I}{\partial \mathcal{F}}\right] - \Psi^T\left[\frac{\partial R}{\partial \mathcal{F}}\right]\right\}\delta \mathcal{F} \qquad (7)$$

The explicit dependence of δI on δW is eliminated by setting

$$\left[\frac{\partial I}{\partial W}\right]^T - \left[\frac{\partial R}{\partial W}\right]^T\Psi = 0 \qquad (8)$$

which is recognized as the adjoint equation to Eq. (5) for the so-called co-state variable Ψ. Once we obtain Ψ by solving the adjoint equation, the needed gradient of I with respect to the geometry change $\delta \mathcal{F}$ is determined by

$$\delta I = G \delta \mathcal{F} \qquad (9)$$

where G is the gradient and

$$G = \left\{\left[\frac{\partial I}{\partial \mathcal{F}}\right] - \Psi^T\left[\frac{\partial R}{\partial \mathcal{F}}\right]\right\} \qquad (10)$$

The derivative terms in the above equation can be easily and cheaply computed even for large numbers of design parameters because we can derive the explicit algebraic dependence of I and R on $\mathcal{F}$. The problem of finding G is then reduced to solving governing flow equation (5) and its adjoint equation (8) each once at a given design cycle independent of the number of design parameters. The adjoint equation is similar to the original flow equation in type and dimensions and thus requires the same level of computational effort for solution.

Since in this study all the cost functions are defined at the exit, we can represent them as an outlet boundary integral

$$I = \int_{B_o} C dB \qquad (11)$$

where C is a scalar function of both flow variables and geometric variables and depends on the definition of the cost function. A weak form of the Euler equations is

$$\int_D \frac{\partial \Psi^T}{\partial \xi_i}(\delta F_i)dD - \int_B \Psi^T(\delta F_i)dB = 0 \qquad (12)$$

where $F_i = S_{ij}f_j$, and $S_{ij} = JK_{ij}^{-1}$, $K_{ij} = \partial x_i/\partial \xi_j$. Adding Eq. (12) to the variation of cost function, we have

$$\delta I = \int_{B_o} \delta C dB - \int_B n_i\Psi^T(\delta F_i)dB + \int_D \frac{\partial \Psi^T}{\partial \xi_i}(\delta F_i)dD \qquad (13)$$

We break δC into two parts, δC_f and δC_g, which represent the flow variation term and the geometric variation term, respectively. Let $\delta C_f = c^T(\delta W)$ on B_i and B_o. Then Eq. (13) can be written as

$$\delta I = \int_{B_i}(c^T - n_iS_{ij}\Psi^T A_j)(\delta W)dB + \int_{B_o}(c^T - n_iS_{ij}\Psi^T A_j)(\delta W)dB$$
$$+ \int_{B_w}[(\delta C_f) - n_iS_{ik}\psi_{k+1}(\delta p)]dB + \int_D \frac{\partial \Psi^T}{\partial \xi_i}S_{ij}A_j(\delta W)dD + \delta I_g \qquad (14)$$

From Eq. (14), we can determine the boundary conditions at the inlet, outlet, and wall. Because of the reversed direction of wave propagation, the method used to determine the boundary condi-

tions of the adjoint equations is different from that used for the Euler equations. Yang et al. [9] discussed the details in their paper. In this paper, the formulations of the adjoint equations, detailed boundary conditions, and gradient are presented in the Appendix.

2.3 A Simple Restagger Method for Annular Cascade. Modifications of the geometric design $\mathcal{F}$ may be directly achieved by moving the grid points on the surface of the blade or other parts of the flow boundary of interest in a numerical computation. However, doing so may violate certain geometric constraints and may not reflect the current practice of turbomachinery blade row design. To simplify the design task, turbine blades have been traditionally represented by a series of profiles stacked together to form a blade. The stacking line is defined along the span of the blade, which joins each of the profiles together through a particular point. This stacking line may move in space, and the profiles may rotate around the stacking line. The stacking line, the blade profile shape at a radial location, and the rotation angle of the blade profile around the stacking line, i.e., the stagger angle, are three major design parameters often used in current practice.

Usually the aerodynamics of blade profiles are designed in two-dimensional space, in a plane that is quasinormal to the spanwise direction. The shape of the profile is redesigned to achieve optimal performance. A major performance indicator is the distribution of pressure or isentropic Mach number over the blade profile surface. The three-dimensional performance is usually checked by considering the blade spanwise distribution of circumferentially averaged aerodynamic parameters. In this way, the performance of the design in the so-called S1 blade-to-blade surface is considered separately from the performance in the meridional S2 stream surface. The design method based on the resolution of S2 and S1 calculations referred in Ref. [16] indeed provides reasonable solution and is widely used in engineering.

In a fully three-dimensional design optimization method, however, a major issue is the linkage of the design space to the aerodynamics analysis space, in particular, where the endwalls are noncylindrical. Typically, the optimization method makes geometrical changes in the CFD mesh, to represent changes in the boundaries of the fluid domain. This is in contrast to the methods used by designers to change the blade shape. To evaluate the effectiveness of the present optimization procedure, it is felt necessary to relate the changes in blade shape to the more traditional design parameters. As mentioned previously, profiles are changed in their respective S1 planes, and the flow in the S2 surface is changed by changes in the stacking line. The hub and tip channel contours are used to recut the blade and form the fluid domain. The application of a profile restagger in the fluid domain for a noncylindrical casing is not so trivial, in particular, at the endwalls. Here, care has to be taken not to change the channel contour when the restagger is applied. Different sophisticated design tools and software systems may be used in practice. However, a simple procedure is presented below to reflect the essence of such a design procedure.

Figure 2 illustrates the transformation of the Kth spanwise blade section of an annular cascade to an auxiliary surface S. O_i is the origin on the turbine rotation axis. l is an auxiliary plane, which includes the stacking line and is parallel to the rotation axis. P_i is the intersection of the Ith x-slice with the auxiliary plane. A_i and B_i are two grid points on the Kth blade section. The blade section is projected onto an auxiliary surface, which is perpendicular to r and goes through P_i. The points C_i and D_i with respect to A_i and B_i satisfy that $\overset{\frown}{P_iA_i} = |P_iC_i|$, $\overset{\frown}{P_iB_i} = |P_iD_i|$, where $\overset{\frown}{P_iA_i}$ and $\overset{\frown}{P_iB_i}$ are the lengths of arcs P_iA_i and P_iB_i.

The first step of this method is to expand the original Kth blade section onto such an auxiliary surface, C_i and D_i are on the same x-slice, and each x-slice of which is perpendicular to r; and $\{r_{P_1}, r_{P_2}, \ldots, r_{P_n}\}$ denotes the array of local radius from the leading edge to the trailing edge of the Kth blade section, corresponding to the array of x-slices $\{x_{P_1}, x_{P_2}, \ldots, x_{P_n}\}$, where n is the num-
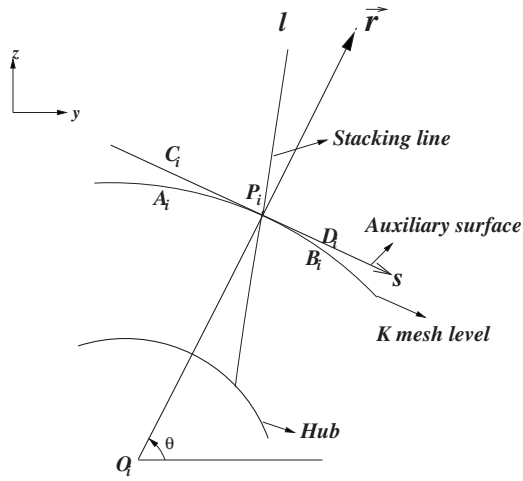
Fig. 2 Transformation of annular cascade onto an auxiliary surface

Fig. 4 Cost function versus design cycle

ber of grid points on each blade surface.

The second step is to rigidly rotate this auxiliary surface about the rotation axis r. The variation of stagger angle equals the rotation angle. After rigid rotation, from the x-coordinate of C_i', which corresponds to C_i, we can determine the new x-slice array signified by $\{x_{P_1'}, x_{P_2'}, \ldots, x_{P'}\}$. Consequently the new radius array is signified by $\{r_{P_1'}, r_{P_2'}, \ldots, r_{P_n'}\}$. The details are shown in Fig. 3. α in Fig. 3 denotes the variation of stagger angle. D_i' is on the same x-slice with C_i'.

The third step is to recover the blade on the auxiliary surface onto the new radial. The new points A_i' and B_i' still satisfy that $\widehat{P_i'A_i'} = |P_i'C_i'|$, $\widehat{P_i'B_i'} = |P_iD_i'|$ and their coordinates are determined by

$$x_{A_i'} = x_{P_i'}, \quad x_{B_i'} = x_{P_i'}$$

$$y_{A_i'} = r_{P_i'} \cos(\theta - |P_i'C_i'|/r_{P_i'}), \quad y_{B_i'} = r_{P_i'} \cos(\theta - |P_i'D_i'|/r_{P_i'})$$

$$z_{A_i'} = r_{P_i'} \sin(\theta - |P_i'C_i'|/r_{P_i'}), \quad z_{B_i'} = r_{P_i'} \sin(\theta - |P_i'D_i'|/r_{P_i'})$$
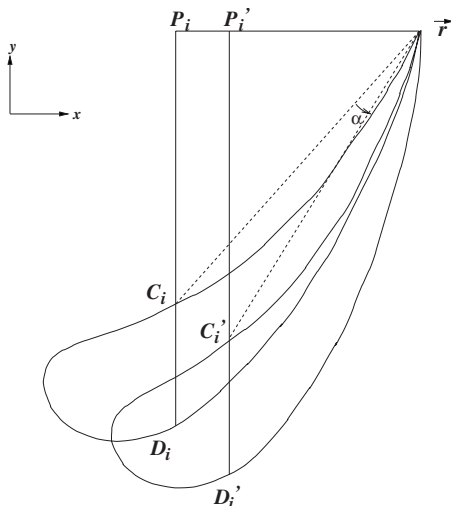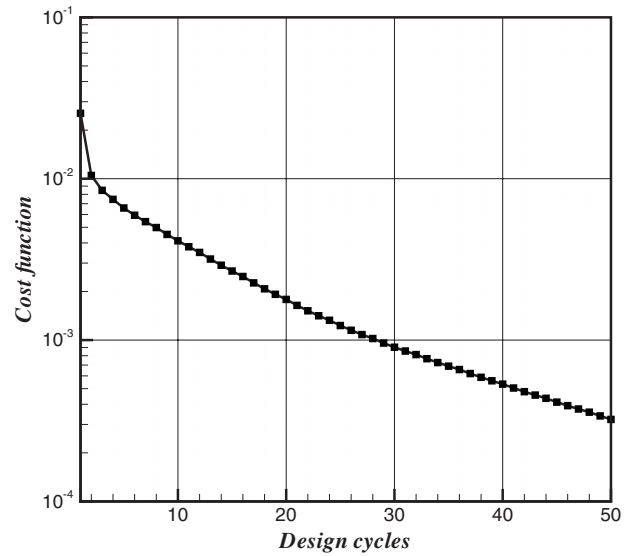

Fig. 3 Rigid rotation of blade section

$$(0 < \theta < \pi)$$

By this method, the blade profile on each section is kept and the axial chord changes.

3 Results and Discussion

As mentioned in Sec. 2, two types of design objectives with different design spaces and constraints are studied. Based on the gradient obtained from the Euler equations and the adjoint equations, the steepest descent method is chosen as the optimization algorithm to ensure the development of design toward the design objectives. The results are presented and discussed in the following subsections 3.1–3.2. The total to static pressure ratio is fixed in all cases.

3.1 Inverse Design to Achieve Given Aerodynamic Load. Flow turning through a blade row is proportional to turbine work with fixed mass flow rate. Similar to the angle of attack for an airfoil and twist of a wing, the stagger angle of a turbomachinery blade profile is a key parameter in determining the flow turning. In the present study, the spanwise stagger angle distribution is chosen as the design parameter. This design case is tested to demonstrate the feasibility of using the adjoint method as an inverse design tool to achieve an arbitrary flow turning distribution by choosing the blade stagger distribution. The inverse design problem is converted into an optimization problem by using the cost function specified in Eq. (1). In order to ensure the same turbine work, the overall mass-averaged flow turning of the target distribution is equal to that of the reference blade for the same mass flow rate.

Figure 4 shows the cost function change versus the design cycle. As discussed earlier, each design cycle consists of one flow solution and one solution of the adjoint equation to obtain the gradient of the cost function with respect to the design parameters, which in this case are the stagger angle distribution along the radial (spanwise) direction. The cost function monotonically decreases with design cycle and is reduced by almost two orders of magnitude within 40 design cycles.

Figure 5 shows the exit flow angle distribution before and after the design. The initial distribution (dotted line) is from the original reference design. To test the ability of the code for inverse design purposes, an arbitrary angle distribution is chosen as the target exit flow angle distribution, which in this case is a straight-line (the solid line in the figure). The placement of the straight-line is such that its one-dimensional average angle is the same as that of
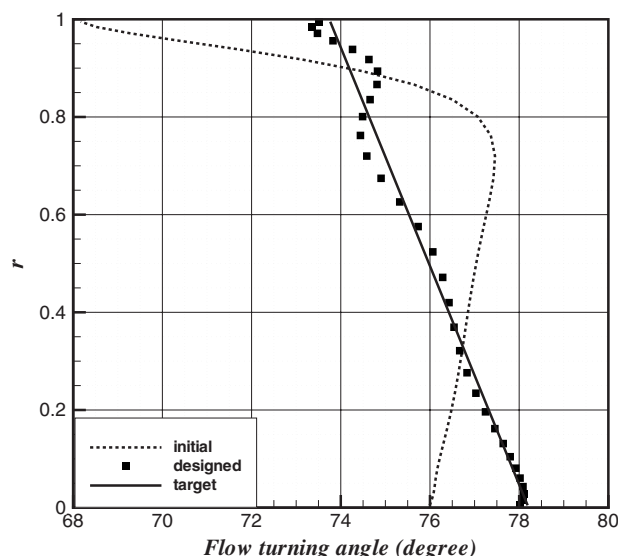
Fig. 5 Exit flow angle before and after design

the initial design. After the 40 design cycles, a flow field is obtained that yields the exit flow angle distribution as shown by the solid squares, which closely approaches the target distribution except near the tip, where the flow appears to have difficulties to follow the straight-line angle distribution. Notice that an inverse design problem is not always well-posed. In other words, there may not be a stagger angle distribution that can yield the specified target flow angle distribution. However, the present optimization method will always find the closest possible solution to the target under the given conditions.

Figure 6 shows the change in stagger angles relative to the original design as needed to produce the designed exit flow angle distribution. This test case demonstrates the ability of the adjoint method for inverse design purposes. In practical applications, the specification of the exit flow angle distribution is left to the judgment of the designer. The choice of the linear distribution is used here for demonstration purposes only.

3.2 Optimization for Maximum Exit Total Pressure. Instead of aiming for an exit angle distribution, maximizing the exit total pressure may be a more effective design strategy, given the
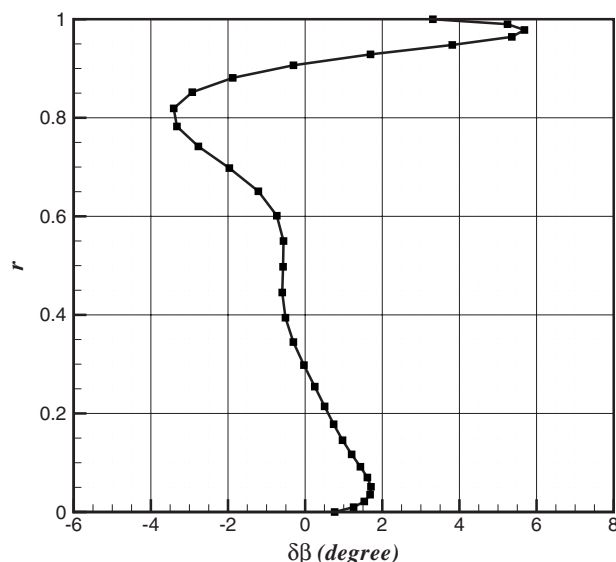

Fig. 6 Designed change in stagger angle distribution

direct link of total pressure loss with blade row performance. There is more than one choice of the cost function. Papadimitriou and Giannakoglou [13] defined it directly as difference of total pressures between the outlet and inlet. The total enthalpy is constant in an adiabatic turbine stator. The entropy generation per unit mass flow rate as defined in Eq. (2) is then a direct measure of total pressure loss.

For this test case, we include in the design space both the spanwise restagger of the blade profiles as in the previous case and the blade profile shape at each spanwise location. The stacking line, however, is still kept unchanged from the reference design. The blade profile is modified by adding a Hicks–Henne shape function at each grid point on the blade surface as was done by Wu et al. [10]. The shape functions are defined as

$$b_i(x) = \sin^4(\pi x^{m_i}), \quad m_i = \ln(0.5)/\ln(x_{M_i}), \quad i = 1, \ldots, N$$

where x is the chordwise coordinate, and x_{M_i} are grid points on the blade surface that are selected as control points of the shape functions. N is the number of control points on each blade surface. Notice that the deformation of each original grid point is along the direction of the mesh line.

Optimization of blade row performance without constraining flow turning across the blade would be physically meaningless just as in the case of minimizing drag of an airfoil in external flow without constraining its lift coefficient to a fixed value. For turbomachinery, an alternative constraint is the mass flow rate. However, specifying both the turning angle and mass flow rate would be an overconstraint since turning angle and mass flow are almost uniquely related across a blade row or a stage. We present below results by imposing the two alternative constraints separately.

3.2.1 Maximum Total Pressure With Fixed Turning. The flow turning at the exit is chosen as a constraint in order to achieve a particular stage characteristic—for example, the stage reaction and stage loading where the design is considered in a stage. This is accomplished by augmenting the cost function in Eq. (2) by the addition of a penalty function as follows:

$$I = s_{\text{gen}} + \Lambda|\bar{\beta} - \bar{\beta}_0|$$

where $\bar{\beta}$ is the mass-averaged flow turning

$$\bar{\beta} = \frac{\int_{B_o} \rho u_j \beta N_j dA}{\int_{B_o} \rho u_j N_j dA}$$

β is the flow turning angle on each cell face at the exit and is defined as the inverse tangent of the ratio of tangential velocity to axial velocity. $\bar{\beta}_0$ is the target mass-averaged exit flow angle, which in this paper is chosen to be that of the original reference design. The penalty weight parameter Λ may be chosen to adjust the tolerance in the enforcement of the constraint. In this study, $\Lambda = 20$.

Figure 7 shows the entropy production, stagnation pressure ratio, and the adiabatic efficiency of the blade row versus design cycle. With 50 design cycles, the adiabatic efficiency is increased by about 0.7 of a percentage point.

Figure 8 shows that the turning angle of flow across the blade row is kept very close to the fixed value during the design process, indicating that the method strictly enforced the desired flow angle constraint. The mass flow rate shown in Fig. 8, however, shows a slight increase. This is brought about by the increased efficiency of the blade row.

Figures 9 and 10 show the total pressure ratio and adiabatic efficiency distribution in the radial direction before and after the redesign. Improvements have been achieved along the whole spanwise direction. Figure 11 indicates that the flow turning angle is decreased near the hub while slightly increased in the 55–85% blade height area. Figure 12 shows the spanwise stagger angle change in addition to blade profile changes needed to achieve this
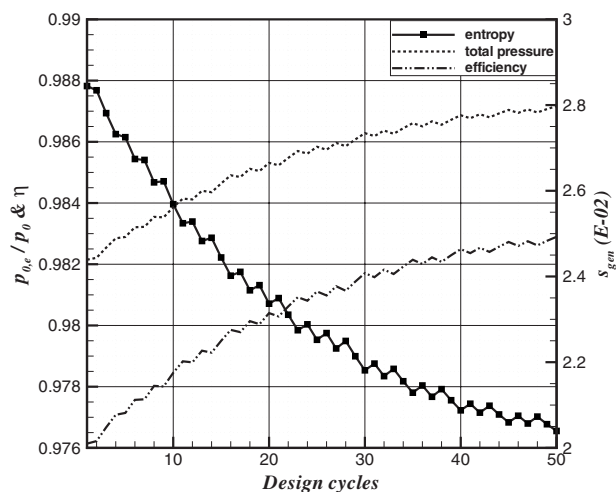
Fig. 7 Total pressure, efficiency, and entropy versus design cycle with turning angle constraint

Fig. 9 Spanwise total pressure distribution

design. The redesign increases the stagger angle across the whole span, especially near the middle. This effectively closes the blade passage.

Figure 13 details the blade profile before and after the redesign at the spanwise grid level $k=17$. Case 1 is the original blade. Case 2 is the redesigned blade with both profile modification and restagger. Case 3 is the blade with only the restagger from Case 2 and Case 4 is that with only the profile modification from Case 2. The flow fields and performance of Cases 3 and 4 are calculated and compared in order to study and compare the effects on the flow by the individual changes in stagger and the blade profile shape, and the combined effect of the two. Table 1 lists the computed dimensionless entropy production, mass flow rate, exit flow angle, and total pressure ratio for the four cases. Figure 14 compares the isentropic Mach number over the blade for the four cases. The original design suffers from a high supersonic suction peak and therefore causes more stagnation pressure loss through the blade row. The high Mach numbers are also seen in the comparisons of the Mach number contours in the blade passage and those on the blade suction surface shown in Figs. 15 and 16, respectively. By restaggering the blade profiles (Case 3), one reduces the suction peak. However, the increased stagger closes the blade passage and consequently reduces the mass flow rate be-
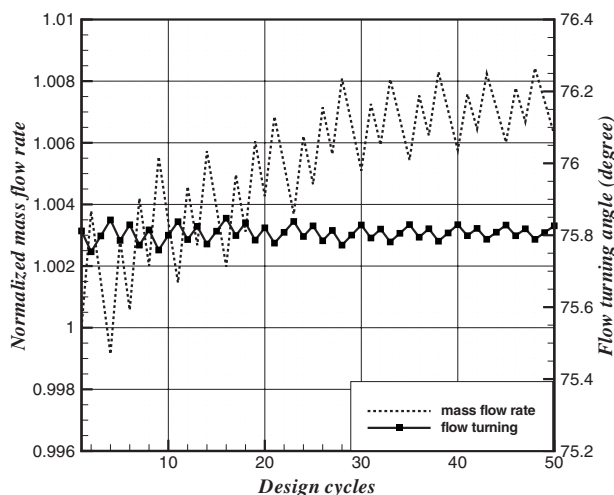
cause most part of the blade passage is already choked in this case. The reduced mass flow rate coupled with increased stagger results in significant flow turning and, in fact, a slight net decrease in total pressure because of the increased entropy generation per unit mass as listed in Table 1. In order to maintain the same turning angle specified in the constraint, the optimizer modifies the blade profile to maintain the same total loading on the blade. By comparing the blade profiles of Case 1 and Case 4 or those of Case 2 and Case 3 in Fig. 13, we see significant thinning of the blade on the suction side. Contrary to the effects of the stagger angle, the change in the blade profile opens the throat of the blade passage and thus leads to increased mass flow rate and increased inlet Mach number. The combination of the restagger and the change in the profiles decreases the suction peak while at the same time increases the loading on the front portion of the blade with the net result of reduced shock loss while maintaining the same flow turning. Figure 17 shows the pitch-averaged total pressure contours in the meridional plane. The redesigned blade shows reduced total pressure loss in the supersonic region of the channel.

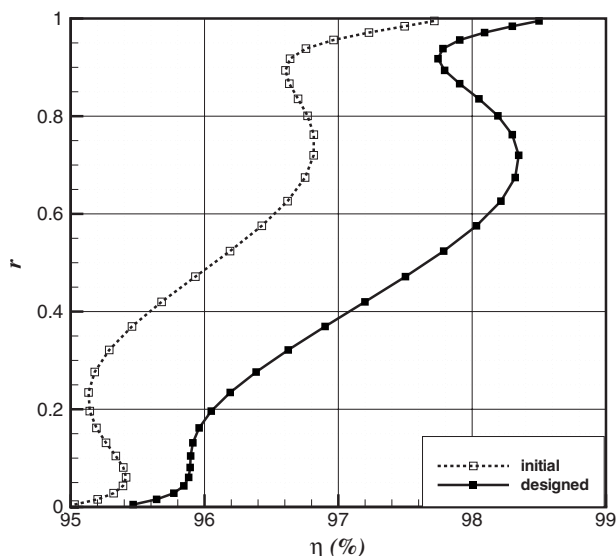Optimization by either restagger or blade profile change alone

Fig. 8 Turning angle and mass flow rate versus design cycle with turning angle constraint

Fig. 10 Spanwise adiabatic efficiency distribution
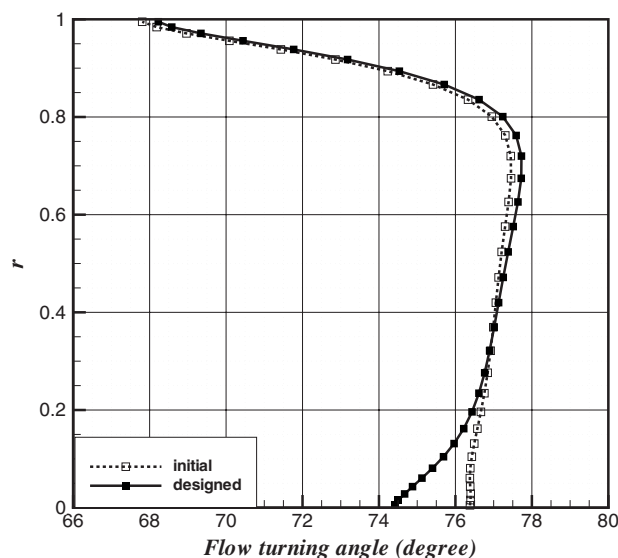
Fig. 11   Spanwise turning angle distribution

Fig. 13   Blade profile at $K=17$

was performed but results showed little gain in performance when a constraint on either mass flow rate or flow turning was imposed. This is understandable from the previous analysis on the effect of the two types of design parameters: stagger angle and blade profile shape. The situation is much similar to that of minimizing drag of an airfoil in external flow by changing the airfoil shape with fixed lift. As the airfoil shape is changed, its angle of attack must usually be adjusted in order to maintain the same lift.

At present the optimization is only performed by using the Euler equations at the design point. In order to assess the performance of the designed blade (Case 2) in real viscous situations and also away from the design point, Navier–Stokes calculations are performed for the initial and the redesigned blades at both design and off-design conditions. Figure 18 compares the computed total pressure ratio and adiabatic efficiency versus the normalized mass flow rate through the blade row. The mass flow rate in the figure is normalized by the choked value of the reference design by the Euler equations. The Navier–Stokes results show reduced total pressure, adiabatic efficiency, and mass flow rate compared with the corresponding Euler solutions as expected due
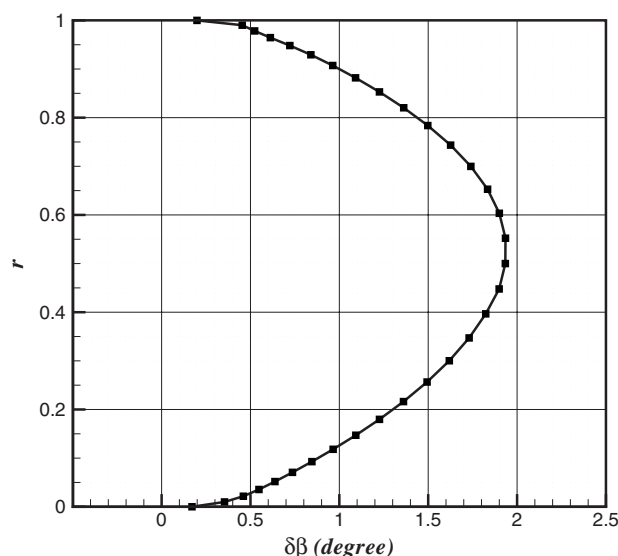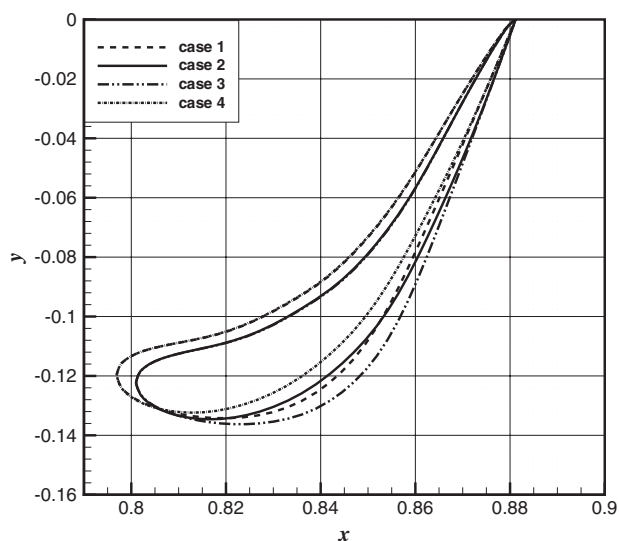
to the inclusion of viscous losses and blockage. Both the Euler and Navier–Stokes results show increased performance and mass flow rate of the redesigned blade compared with the reference blade. Because of the overall better behavior of the flow field of the redesigned blade, the relative reduction in mass flow rate due to viscous blockage revealed by the Navier–Stokes computations is also less for the redesigned blade. Figure 19 shows the improvements in adiabatic efficiency of the redesigned blade row based on the Euler and the Navier–Stokes evaluations. Both calculations reveal performance gains over the whole range of computed operating pressure ratios even though the design optimization was performed at the design point corresponding to an exit isentropic

Table 1   The effects of stagger and blade shape

Case	s_{gen} $(\times 10^{-2})$	$\dot{m}$ $(\times 10^{-3})$	β (deg)	$p_{0,e}/p_0$
1	2.844	7.268	75.812	0.9821
2	2.040	7.314	75.826	0.9872
3	2.891	6.685	76.835	0.9819
4	1.943	7.895	74.779	0.9878

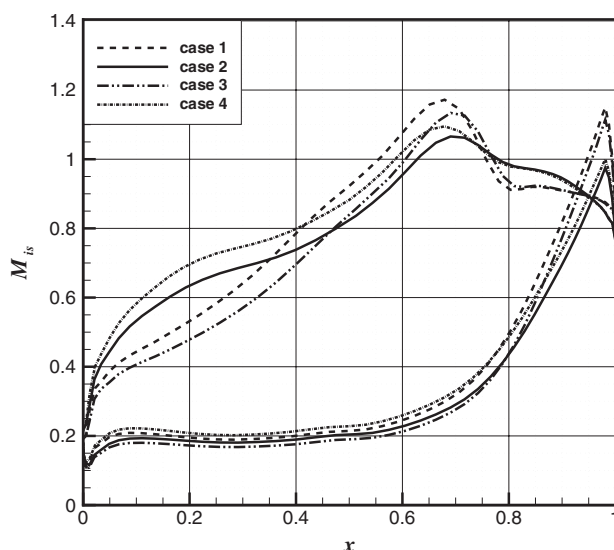**Fig. 12   Spanwise distribution of stagger angle change**

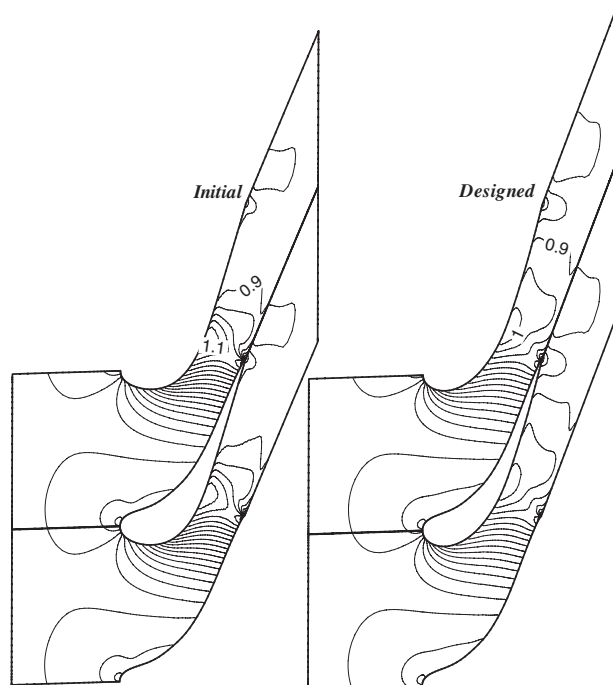**Fig. 14   Blade isentropic Mach number distribution at $K=17$**

Fig. 15   Mach number contours at K=17

Mach number of 1.16. The difference between the adiabatic efficiency gains predicted by the Navier–Stokes and the Euler evaluations is small (less than 0.1 percentage point) and almost a constant except near the very low back pressure point where the flow is fully choked. This is not surprising for the type of steam turbine blades as considered here for the following three reasons. First, the overall pressure gradient in a turbine blade row is favorable. Thus, viscous separation does not happen easily in a reasonably well designed blade row. The additional loss due to viscous effect is mostly due to wall skin frictional loss, which stays relatively constant. Second, the flow in such a turbine is mostly supersonic and therefore losses are mostly from shocks or strong compression waves, which the Euler equations can accurately resolve. Third, the low-pressure steam turbine blades have high aspect ratios. Therefore, endwall and secondary flow losses are small. As the back pressure is decreased to approach choking, the difference in efficiency gain between the viscous and inviscid predictions
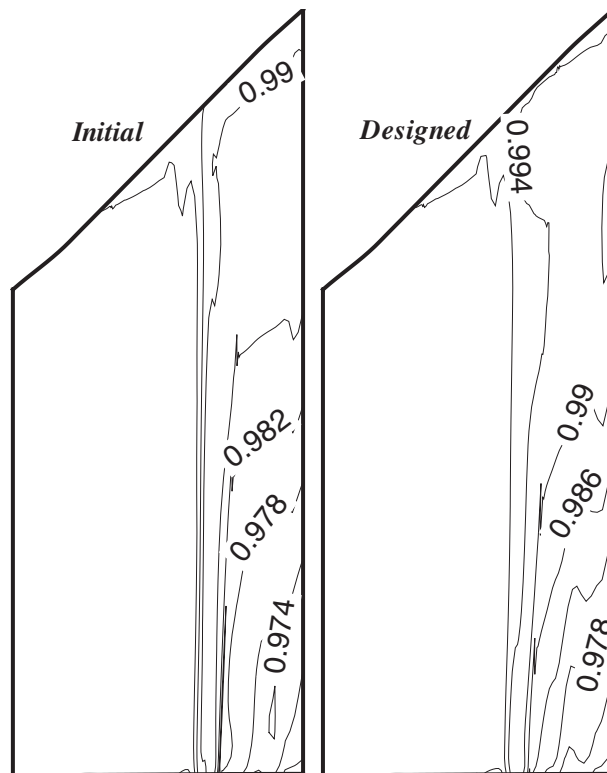

Fig. 17   Pitch-averaged total pressure contours

becomes negligible because the losses are dominated by shocks.

Despite the remarkable success of the above design optimization based on the Euler equations, the need is recognized for a Navier–Stokes based optimization method for problems where viscous effects may be significant. Future work will extend the adjoint method to the Navier–Stokes equations.

Both the Euler and Navier–Stokes calculations show consistent performance gains over the complete off-design range by the design that is optimized only at the design condition and as such we can only claim optimality at the design condition. For this test case of steam turbine blades, this conclusion is not surprising because of the roundness of the leading edge, which ensures good tolerance to off-design inflow angles. To add robustness in the
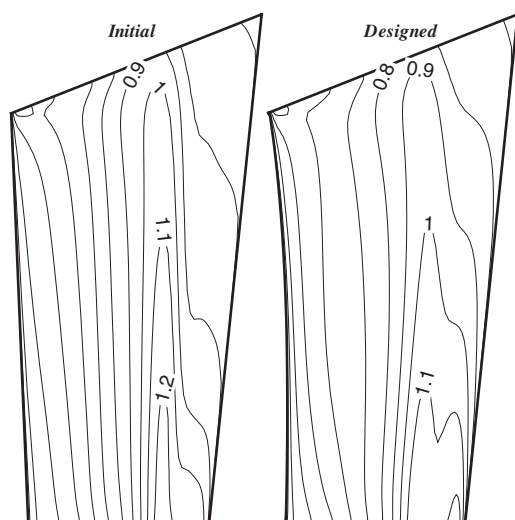

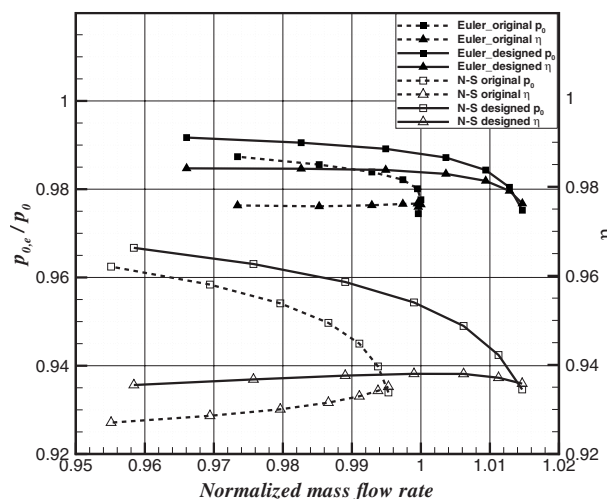**Fig. 16   Mach number contours on blade suction surface**

Fig. 18   Comparisons of total pressure ratio and efficiency of both reference and designed blades
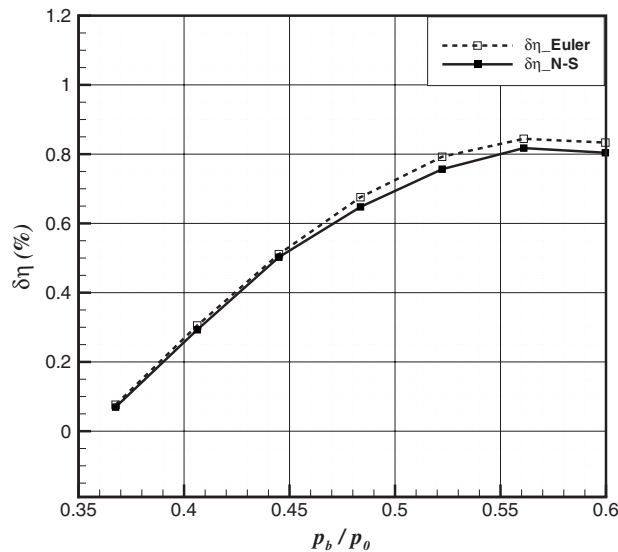
Fig. 19 Variations of adiabatic efficiency gains predicted by the Euler and NS flow calculations

future one needs to consider multipoint design, which can be included in the present method by using a weighted cost function. Nevertheless, a check of the designed blade at off-design conditions like the one performed here serves as a good practice.

3.2.2 Maximum Total Pressure With Fixed Swallowing Capacity. We consider optimization under the constraint of fixed mass flow rate instead of fixed turning angle. This can be achieved by choosing the following cost function that contains a penalty function on the mass flow deviation from the specified design mass flow rate:

$$I = s_{\text{gen}} + \Lambda |\dot{m} - \dot{m}_0|$$

where $\dot{m}_0$ is the specified mass flow rate and $\dot{m}$ is the computed mass flow rate during the design.

Figure 20 shows the entropy production, total pressure ratio, and adiabatic efficiency versus design cycle for the optimization. The general behavior of the optimization process is similar to that when the turning angle is used as the constraint. Figure 21 shows that in this case the mass flow rate is indeed kept to be almost constant and the turning angle slightly increased. Computations show that it is not possible to improve the blade performance if
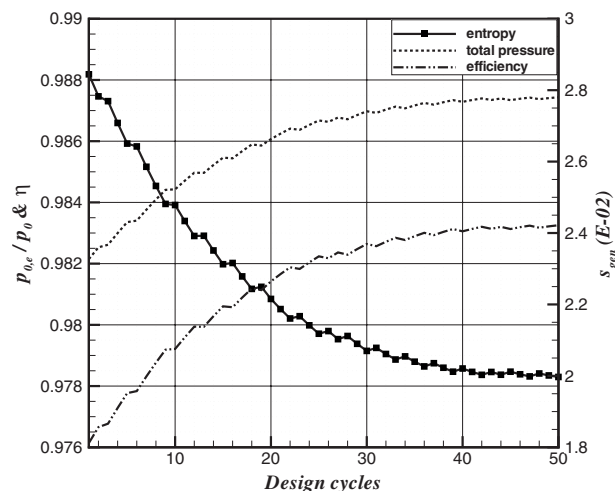

Fig. 20 Total pressure, efficiency, and entropy versus design cycle with mass flow constraint
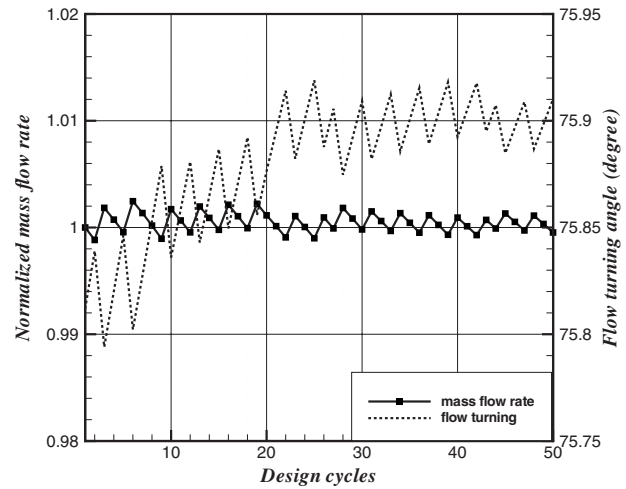

Fig. 21 Turning angle and mass flow rate versus design cycle with mass flow constraint

both the flow angle and the mass flow rate must be kept unchanged—this is somewhat intuitive, as the blade loading and swallowing capacity constrain the performance to a certain level. An improved blade design will either increase the flow turning while maintaining the same mass flow rate or increase the mass flow rate if the turning angle is kept the same. Figure 22 shows the stagger angle change in the redesigned blade. The general behavior is the same as that shown in Fig. 12.

4 Conclusions

An efficient design optimization method based on the adjoint-equation approach is presented for turbomachinery blade row design. Gradient information of the cost functions is obtained by solving the Euler equations and the corresponding adjoint equations only once, independent of the number of design parameters. The method is demonstrated to perform both inverse design and direct optimization of performance parameters with constraints for a high-speed steam turbine nozzle blade row. Care is taken to apply appropriate thermodynamic constraints, to ensure that the observed design improvements are valid in a typical design process. In the inverse design case, the designer may specify a desired spanwise distribution of exit flow angle. The design optimi-
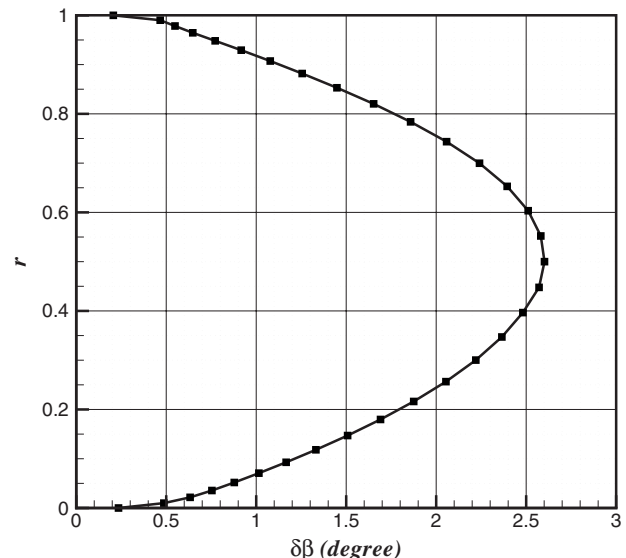

Fig. 22 Spanwise distribution of stagger angle change

zation code successfully restaggers the blade profiles to achieve the exit flow angle within a few tens of design cycles. In the direct optimization test cases, the mass-averaged entropy production across the blade row is chosen as the cost function. The optimization minimizes this cost function by modifying the blade profiles and restaggering the profiles. Constraints are imposed by adding a penalty term in the cost function. Two different constraints are considered in the investigations. The first is to maintain a fixed mass-averaged exit flow angle. The second is to maintain a fixed total mass flow rate. The optimization increases the adiabatic efficiency of the blade by about 0.6 of a percentage point with either fixed (with less than 0.1% error) turning angle or fixed mass flow rate. Examination of the flow field shows that this gain in efficiency is obtained by reducing the supersonic suction peak in the nozzle passage through a combination of profile modification and restaggering of the blade profiles. Restaggering or blade profile change alone is not sufficient to produce significantly improved design without violating the thermodynamic constraints. When the blade profile is changed, restaggering is necessary to maintain the overall loading of the blade such that the turning angle constraint is satisfied.

Acknowledgment

Nomenclature

a = speed of sound
A_i = Jacobian matrices, $A_i = \partial f_i / \partial W$
B = boundaries of the ξ domain
c_p = constant pressure specific heat
D = the computational domain (ξ domain)
f_i = inviscid flux
G = gradient for optimization
I = cost function
K_{ij} = transformation functions between the physical domain and the computational domain, $K_{ij} = \partial x_i / \partial \xi_j$
$\dot{m}$ = mass flow rate
M_{is} = isentropic Mach number
n_i = unit normal vector in the ξ domain, pointing outward from the flow field
N_j = unit normal vector in the physical domain, pointing outward from the flow field
$p_{0,e}$ = exit total pressure
R_g = gas constant
s_{gen} = entropy generation per unit mass flow rate
s = entropy, $s = -R_g \ln p_{0,e}/p_0$
u_t = tangential velocity
u_x = axial velocity
W = conservative flow variables, $W = \{\rho, \rho u, \rho v, \rho w, \rho E\}^T$
x_i = coordinates in the physical domain
$\bar{\beta}$ = mass-averaged exit flow turning angle
Λ = weight of the penalty function
ξ_i = coordinates in the computational domain
Ψ = co-state variables, $\Psi = \{\psi_1, \psi_2, \psi_3, \psi_4, \psi_5\}^T$

Appendix: Boundary Conditions, Adjoint Equations, and Variation of Cost Functions

1 Boundary Conditions of Flow Solver

1.1 Inlet Boundary Conditions. The total pressure p_0, total temperature T_0, and the two inflow angles are specified.

1.2 Outlet Boundary Conditions. The back pressure p is specified.

1.3 Inviscid Wall Boundary Conditions. The normal velocity component is zero as follows:

$$U \cdot N = 0$$

1.4 Periodic Boundary Conditions.

$$w_{i,B2} = w_{i,B1}, \quad i = 1,2,5$$

$$w_{3,B2} = w_{3,B1} \cos \theta - w_{4,B1} \sin \theta$$

$$w_{4,B2} = w_{3,B1} \sin \theta + w_{4,B1} \cos \theta$$

where $B1$ and $B2$ are two periodic boundaries, and θ is the pitch angle of annular cascade.

2 Adjoint Equations.
The final expression of the adjoint equations in unsteady form is

$$\frac{\partial \Psi}{\partial t} - A_i^T \frac{\partial \Psi}{\partial x_i} = 0 \tag{A1}$$

3 Inlet Boundary Conditions of Adjoint Equations: ($n_1 = -1$, $n_2 = 0$, $n_3 = 0$)

$$\delta C_f = 0, \quad c^T = 0$$

The details of the inlet boundary condition are shown by Wu and Liu [11].

4 Outlet Boundary Conditions of Adjoint Equations: ($n_1 = 1$, $n_2 = 0$, $n_3 = 0$)

4.1 Inverse Design Case. The cost function of the inverse design case can also be written in discrete form

$$I = \sum_{k=1}^{KL} \frac{1}{2} [\bar{\beta}(k) - \bar{\beta}_0(k)]^2 \tag{A2}$$

where KL is the number of flow turning's components. The outlet boundary conditions are

$$(A_{j+1,k}^* + A_{1,k}^* \bar{K}_{j+1}) \psi_k = c_{j+1} + \bar{K}_{j+1} c_1, \quad j = 1,2,3,4 \tag{A3}$$

where $A^* = n_i S_{ij} A_j$ and

$$\bar{K}_1 = 0, \quad \bar{K}_2 = \frac{2u_1}{u_j u_j}, \quad \bar{K}_3 = \frac{2u_2}{u_j u_j}, \quad \bar{K}_4 = \frac{2u_3}{u_j u_j}, \quad \bar{K}_5 = -\frac{2}{u_j u_j} \tag{A4}$$

$$\begin{Bmatrix} c_1 \\ c_2 \\ c_3 \\ c_4 \\ c_5 \end{Bmatrix} = \begin{Bmatrix} 0 \\ (\bar{\beta}(k) - \bar{\beta}_0(k))\left(-\frac{\beta}{m_f} S_{11} + \frac{\bar{\beta}_k}{m_f} S_{11} - \frac{\rho u_k}{m_f} S_{1k} g_2\right) \\ (\bar{\beta}(k) - \bar{\beta}_0(k))\left(-\frac{\beta}{m_f} S_{12} + \frac{\bar{\beta}_k}{m_f} S_{12} - \frac{\rho u_k}{m_f} S_{1k} g_3\right) \\ (\bar{\beta}(k) - \bar{\beta}_0(k))\left(-\frac{\beta}{m_f} S_{13} + \frac{\bar{\beta}_k}{m_f} S_{13} - \frac{\rho u_k}{m_f} S_{1k} g_4\right) \\ 0 \end{Bmatrix}$$

$$g_2 = \frac{1}{\rho} \frac{-u_t}{u_x^2 + u_t^2}, \quad g_3 = \frac{1}{\rho} \frac{u_x \sin \theta}{u_x^2 + u_t^2}, \quad g_4 = \frac{1}{\rho} \frac{1 - u_x \cos \theta}{u_x^2 + u_t^2}$$

4.2 Optimal Design Case. The outlet boundary conditions are

$$(A^*_{j+1,k} + A^*_{1,k}\bar{K}_{j+1})\psi_k = \text{sign}(\bar{\beta} - \bar{\beta}_0)\Lambda(c_{\beta,j+1} + \bar{K}_{j+1}c_{\beta,1}) + c_{s,j+1}$$
$$+ \bar{K}_{j+1}c_{s,1}, \quad j = 1,2,3,4$$

where

$$\begin{Bmatrix} c_{s,1} \\ c_{s,2} \\ c_{s,3} \\ c_{s,4} \\ c_{s,5} \end{Bmatrix} = \begin{Bmatrix} -\dfrac{1}{m_f}c_p u_j S_{1j} \\ \dfrac{1}{m_f}(s - s_{\text{gen}})S_{11} \\ \dfrac{1}{m_f}(s - s_{\text{gen}})S_{11} \\ \dfrac{1}{m_f}(s - s_{\text{gen}})S_{11} \\ 0 \end{Bmatrix}$$

$$\begin{Bmatrix} c_{\beta,1} \\ c_{\beta,2} \\ c_{\beta,3} \\ c_{\beta,4} \\ c_{\beta,5} \end{Bmatrix} = \begin{Bmatrix} 0 \\ \dfrac{1}{m_f}((\beta - \bar{\beta})S_{11} + \rho u_j S_{1j}g_2) \\ \dfrac{1}{m_f}((\beta - \bar{\beta})S_{12} + \rho u_j S_{1j}g_3) \\ \dfrac{1}{m_f}((\beta - \bar{\beta})S_{13} + \rho u_j S_{1j}g_4) \\ 0 \end{Bmatrix}$$

5 Inviscid Wall Boundary Conditions

$$N_k\psi_{k+1} = 0, \quad k = 1,2,3 \tag{A5}$$

6 Resultant Variation of Cost Functions

$$\delta I = \delta I_g = \int_B (\delta C_g)dB + \int_{B_W} n_i(\delta S_{ij})\Psi^T \bar{f}_j dB - \int_D \Psi^T \frac{\partial(\delta S_{ij}f_j)}{\partial \xi_i}dD$$
$$\tag{A6}$$

where

$$\bar{f}_j = \begin{Bmatrix} \rho u_j \\ \rho u_1 u_j \\ \rho u_2 u_j \\ \rho u_3 u_j \\ \rho u_j E \end{Bmatrix}$$

References

[1] Jameson, A., 2003, "Aerodynamic Shape Optimization Using the Adjoint Method," Lectures at the von Karman Institute.

[2] Samad, A., and Kim, K. Y., 2008, "Multiple Surrogate Modeling for Axial Compressor Blade Shape Optimization," J. Propul. Power, **24**(2), pp. 301–310.

[3] Jang, C. M., Li, P., and Kim, K. Y., 2005, "Optimization of Blade Sweep in a Transonic Axial Compressor Rotor," JSME Int. J., **48**(4), pp. 793–801.

[4] Hager, J. O., Eyi, S., and Lee, K. D., 1993, "Design Efficiency Evaluation for Transonic Airfoil Optimization: A Case for Navier-Stokes Design," AIAA Paper No. 93-3112.

[5] Jameson, A., 1988, "Aerodynamic Design Via Control Theory," J. Sci. Comput., **3**(3), pp. 233–260.

[6] Jameson, A., 1995, "Optimum Aerodynamic Design Using CFD and Control Theory," AIAA Paper No. 95-1729.

[7] Kim, S., Alonso, J. J., and Jameson, A., 2004, "Multi-Element High-Lift Configuration Design Optimization Using Viscous Continuous Adjoint Method," J. Aircr., **41**(5), pp. 1082–1097.

[8] Dreyer, J. J., and Martinelli, L., 2001, "Hydrodynamic Shape Optimization of Propulsor Configurations Using a Continuous Adjoint Approach," AIAA Paper No. 2001-2580.

[9] Yang, S., Wu, H., and Liu, F., 2003, "Aerodynamic Design of Cascades by Using an Adjoint Equation Method," AIAA Paper No. 2003-1068.

[10] Wu, H., Yang, S., and Liu, F., 2003, "Comparison of Three Geometric Representations of Airfoils for Aerodynamic Optimization," AIAA Paper No. 2003-4095.

[11] Wu, H., and Liu, F., 2005, "Aerodynamic Design of Turbine Blades Using an Adjoint Equation Method," AIAA Paper No. 2005-1006.

[12] Wu, H., 2005, "Aerodynamic Optimization of Internal and External Flows Using the Adjoint-Equation Method," Ph.D. thesis, Department of Mechanical and Aerospace Engineering, University of California, Irvine, Irvine, CA.

[13] Papadimitriou, D. I., and Giannakoglou, K. C., 2006, "A Continuous Adjoint Method for the Minimization of Losses in Cascade Viscous Flows," AIAA Paper No. 2006-49.

[14] Wang, D., and He, L., 2010, "Adjoint Aerodynamic Design Optimization for Blades in Multi-Stage Turbomachines: Part I—Methodology and Verification," ASME J. Turbomach. **132**, p. 021011.

[15] Wang, D., He, L., Wells, R., and Chen, T., 2010, "Adjoint Aerodynamic Design Optimization for Blades in Multi-Stage Turbomachines: Part II—Validation and Application," ASME J. Turbomach. **132**, p. 021012.

[16] Havakechian, S., and Greim, R., 1999, "Aerodynamic Design of 50 Percent Reaction Steam Turbines," Proc. Inst. Mech. Eng., Part C: J. Mech. Eng. Sci., **213**(1), pp. 1–25.